Mice doubly deficient for the Polycomb Group genes *Mel18* and *Bmi1* reveal synergy and requirement for maintenance but not initiation of Hox gene expression

Takeshi Akasaka[1], Maarten van Lohuizen[2], Nathalie van der Lugt[3], Yoko Mizutani-Koseki[1], Masamoto Kanno[4], Masaru Taniguchi[5], Miguel Vidal[6], Mark Alkema[3], Anton Berns[3] and Haruhiko Koseki[1,*]

[1]Department of Molecular Embryology, Graduate School of Medicine, Chiba University, 1-8-1 Inohana, Chuo-ku, Chiba 260-8670, Japan
[2]Division of Molecular Carcinogenesis, The Netherlands Cancer Institute, Plesmanlaan 121, 1066 CX Amsterdam, The Netherlands
[3]Division of Molecular Genetics, The Netherlands Cancer Institute, Plesmanlaan 121, 1066 CX Amsterdam, The Netherlands
[4]Department of Immunology and Parasitology, School of Medicine, Hiroshima University, Kasumi 1-2-3, Minami-ku, Hiroshima, Japan
[5]CREST and Department of Molecular Immunology, Graduate School of Medicine, Chiba University, 1-8-1 Inohana, Chuo-ku, Chiba 260-8670, Japan
[6]Centro de Inverstigaciones Biologicas, Verazques 144, 28006 Madrid, Spain
*Author for correspondence (e-mail: koseki@med.m.chiba-u.ac.jp)

SUMMARY

Polycomb group genes were identified as a conserved group of genes whose products are required in multimeric complexes to maintain spatially restricted expression of Hox cluster genes. Unlike in *Drosophila*, in mammals Polycomb group (PcG) genes are represented as highly related gene pairs, indicative of duplication during metazoan evolution. *Mel18* and *Bmi1* are mammalian homologs of *Drosophila Posterior sex combs*. Mice deficient for *Mel18* or *Bmi1* exhibit similar posterior transformations of the axial skeleton and display severe immune deficiency, suggesting that their gene products act on overlapping pathways/target genes. However unique phenotypes upon loss of either Mel18 or Bmi1 are also observed. We show using embryos doubly deficient for *Mel18* and *Bmi1* that Mel18 and Bmi1 act in synergy and in a dose-dependent and cell type-specific manner to repress Hox cluster genes and mediate cell survival of embryos during development. In addition, we demonstrate that *Mel18* and *Bmi1*, although essential for maintenance of the appropriate expression domains of Hox cluster genes, are not required for the initial establishment of Hox gene expression. Furthermore, we show an unexpected requirement for Mel18 and Bmi1 gene products to maintain stable expression of Hox cluster genes in regions caudal to the prospective anterior expression boundaries during subsequent development.

Key words; Polycomb, Mel18, Bmi1, Hox, Apoptosis, Mouse

INTRODUCTION

The Polycomb group (PcG) genes were first identified in *Drosophila* as a group of genes required for maintenance of stable repression of Hox cluster genes during development (Paro, 1995; Pirotta, 1997). Biochemical and immunohistochemical analyses indicate that *Drosophila* PcG gene products function as large multimeric protein complexes that are thought to act by changing local chromatin structure (Paro, 1995; Pirotta, 1997). Synergistic genetic interactions between mutant alleles of different *Drosophila* PcG genes indicate their capability to affect expression of Hox genes in gene dose-dependent manner and are in line with the action of PcG gene products in multimeric protein complex (Franke et al., 1992; Jurgens, 1985; Shao et al., 1999).

An increasing number of mammalian genes structurally and functionally related to *Drosophila* PcG genes have been identified. The PcG gene products form part of two different complexes. One contains Eed (ortholog of *Drosophila extra sex combs*), and Enx1 and Enx2 (homologs of *Drosophila enhancer of zeste*) (Schumacher et al., 1996; Hobert et al., 1996; Laible et al., 1997; Sewalt et al., 1998; van Lohuizen et al., 1998). Interestingly, Eed has been shown to interact with histone deacetylases (van der Vlag and Otte, 1999). The second complex includes the products of the highly related gene pairs *Mel18* (*Zfp144* – Mouse Genome Informatics) and *Bmi1*; *M33/Cbx2* and *HPc2/Mpc2* (*Cbx4* – Mouse Genome Informatics); *rae28/Mph1* and *Hph2/Mph2* (*Edr2* – Mouse Genome Informatics); and Ring1A (*Ring1* – Mouse Genome Informatics) and Ring1B (*Rnf2* – Mouse Genome Informatics;

Tagawa et al., 1990; van Lohuizen et al., 1991a; Pearce et al., 1992; Satijn et al., 1997; Nomura et al., 1994; Gunster et al., 1997; Hemenway et al., 1998; Schoorlemmer et al., 1997). This complex is similar to the Polycomb repressive complex 1 (PRC1) recently identified in *Drosophila*. None of the known components of this complex is known to associate with histone deacetylases (Shao et al., 1999; Strouboulis et al., 1999; van der Vlag and Otte, 1999; Satijn and Otte, 1999; van Lohuizen, 1999; Gebuhr et al., 2000).

The two PcG complexes seem to differ in their functional properties in vivo. This is best illustrated by loss-of-function experiments in mice, for example during early hemopoiesis, where loss of *eed* or *Bmi1* has opposing effects on cell survival and proliferation (Jacobs et al., 1999b; Lessard et al., 1999). Mice deficient for individual components of the PRC1-like complex display anterior shifts in the expression boundaries of Hox cluster genes in the paraxial mesoderm and neural tube and, in general, show characteristic posterior transformations of the axial skeleton. In addition, these mice invariably display severe combined immunodeficiency, owing to increased apoptosis and lack of proliferative responses of hemopoeietic cells (van der Lugt et al., 1994; Akasaka et al., 1997; Coré et al., 1997; Takihara et al., 1997; Katoh-Fukui et al., 1998; Jacobs et al., 1999a).

In contrast to these relatively mild phenotypes, a mouse line deficient in the product of the *eed* gene die at gastrulation (5-6 days postcoitus (dpc)) with severe patterning defects. Interestingly, an *eed* hypomorphic mutant did survive until birth and displayed skeletal defects reminiscent of those found in mice lacking components of the mouse PRC1 complex (Schumacher et al., 1996). The apparent difference in severity between the respective null mutant mice, together with the distinct biochemical properties and opposite effects in hemopoiesis, could suggest that the two types of PcG complexes regulate separate target genes. Another possibility is that the mild phenotypes of mice deficient in mouse PRC1 components reflects a functional redundancy between the highly related gene pairs. In this respect, it is relevant to note that *eed* is an exception to the otherwise duplicated PcG genes, in that it appears to be represented in mice and man as a unique gene.

The currently best studied PRC1-related PcG genes in mammals are *Mel18* and *Bmi1*. Mel18 and Bmi1 proteins show high structural resemblance in their N-terminal RING finger and helix-turn-helix (HTH) domains (van Lohuizen et al., 1991b). Both Mel18 and Bmi1 function as transcriptional repressors and are able to bind to the same set of mammalian PcG proteins (Kanno et al., 1995; Alkema et al., 1997; Gunster et al., 1997; Hemenway et al., 1998; Satijn and Otte, 1999; T. A. and H. K., unpublished). This suggests the possibility of a functional redundancy between these PcG proteins, which is consistent with very similar posterior transformations of the axial skeleton and severe combined immunodeficiency, which are due to impaired responsiveness to lymphokines such as interleukin 7, observed in *Mel18*- and *Bmi1*-deficient mice. However, differences in function between *Mel18* and *Bmi1* are also suggested by unique phenotypes observed in the respective null mutant mice, such as neurological defects in *Bmi1*−/− mice versus defects in smooth muscle of the colon in *Mel18*−/− mice (Akasaka et al., 1996; van der Lugt et al., 1994). This is reflected in both overlapping changes of Hox gene expression boundaries as well as uniquely affected Hox genes in *Mel18*-

and *Bmi1*-deficient mice (Akasaka et al., 1997; van der Lugt et al., 1994; van der Lugt et al., 1996).

To further investigate the potential redundancy between related PcG genes and the function of PcG complexes in vivo, we describe the generation and analysis of embryos lacking both *Mel18* and *Bmi1* genes. We show gene dosage effects of *Mel18* and *Bmi1* on survival of embryos and embryonic cells, regulation of Hox gene repression and skeletal development. These results demonstrate a requirement for Mel18 and Bmi1 during embryonic development. We further show that Mel18 and Bmi1 proteins are essential for maintenance, but not the establishment of the appropriate expression domains of Hox genes. Finally, we also show that both Mel18 and Bmi1 are required to maintain appropriate expression level of some Hox genes and of *Evx1*.

MATERIALS AND METHODS

Mice

$Mel18^{+/-};Bmi1^{+/-}$ mice were backcrossed onto a C57BL/6 background three or four times and mated to generate double homozygotes. Genotypes of the double mutants were determined by PCR analysis of tail, kidney or yolk sac DNA using oligonucleotide previously described (Akasaka et al., 1996; van der Lugt et al., 1996). The presence of a vaginal plug at noon of the next day was considered day 0.5 dpc.

Skeletal analysis

Skeletal preparations were made from perinatal mice and cleared skeletons were analyzed under an stereomicroscope as described previously (Kessel and Gruss, 1991).

In situ hybridization

In situ hybridization on tissue sections and whole mount in situ hybridization were performed as described (Kessel and Gruss, 1991; Wilkinson, 1992). For whole-mount in situ hybridization, we used maleic acid buffer (0.5 M maleic acid, 0.15M NaCl (pH7.5)) instead of TBST for washes after antibody incubation. We used riboprobes for *Hoxb3*, *Hoxb6*, *Hoxc6, Hoxd4, Evx1, Shh* and *Pax1*.

Electron microscopic analysis

9.5 dpc embryos were dissected, fixed for 6 hours in 2% glutaraldehyde in phosphate-buffered saline (PBS), washed with PBS and transferred into 50% ethanol for 15 minutes. For observation of the samples, we used a various pressure scanning electron microscopy (S-2380N, Hitachi, Japan) equipped with a cooling stage unit.

Detection of programmed cell death

9.5 dpc embryos were dissected, fixed for 6 hours in 4% paraformaldehyde in PBS, and embedded in paraffin wax. Sections were cut at 7 μm and placed onto 3-aminopropryltriethoxysilane-coated slides. The in situ TdT-mediated dUTP-fluorescein-labeled nick end labeling (TUNEL) was performed on paraffin sections using cell death detection kits (Boehringer Mannheim) with slight modifications. The TUNEL reaction mixture was diluted in threefold with 30 mM Tris (pH 7.2), 140 mM cacodylic acid and 1 mM cobalt chloride.

Quantitative RT-PCR and western blot analysis

The competitor DNA fragments for the Hoxb6 and β-actin gene transcripts were generated by PCR by introducing 25 base pairs (bp) and 55 bp deletions, respectively. The following primers were used; 5′-AAAGACTCCCTGACCCCAGAC-3′ and 5′-TCCCGAGCTAA-GACAAGACTACAAATAGAACTTTGTTCTCTTCTG-3′ for *Hoxb6*,

and 5′-GAGAGGGAAATCGTGCGTGAGCCGCATCCTCTTCCTC-3′, 5′-ACATCTGCTGGAAGGTGGAC-3′ for the β-actin gene. Serial dilutions of competitor DNA fragments were added to the PCR reactions. The amounts of cDNA were first normalized by competitive PCR for β-actin gene transcripts and then the same amount of cDNA was subjected to competitive PCR for *Hoxb6* transcripts. For RT-PCR analysis, the following combinations of primers were used to detect the following transcripts:

5′-AAAGACTCCCTGACCCCAGAC-3′ and 5′-TCCCGAGCTA-AGACAAGACTACAA-3′ for *Hoxb6*;

5′-GAGAGGGAAATCGTGCGTGA-3′ and 5′-ACATCTGCTGG-AAGGTGGAC-3′ for β-actin;

5′-GCACGCTTCTCTCGGAGGTT-3′ and 5′-CCGCCGCTTGTC-CTTGTT-3′ for *Hoxd13*;

5′-CTTGGTCACTGTGAGGATTCAG-3′ and 5′-TCCGCTGCAG-ACAGACTGGCCAG-3′ for *p19arf*;

5′-GAGGCGGATTTAGCTCTGCTC-3′ and 5′-TCCGCTGCAGA-CAGACTGGCCAG-3′ for *p16*;

5′-TCGCTACCGTCGTGACTTC-3′ and 5′-AAACAGAGGTCG-CATGCTG-3′ for *Bcl2*;

5′-TGGTCGACTTTCTCTCCTAC-3′ and 5′-AGAGATCCACAA-AGATGTCC-3′ for Bcl-X$_L$ (*Bcl2l* – Mouse Genome Informatics);

5′-ACAGATCATGAAGACAGGGG-3′ and 5′-CAAAGTAGAAG-AGGGCAACC-3′ for *Bax*; and

5′-GAGCCGAGTGAGCAGGAAGA-3′ and 5′-CCCCAGTTATG-ACAGGACAGCA-3′ for *Bad*. To avoid product saturation, PCR reactions were limited to 28 cycles.

For western blot analyses, the following antibodies were used according to the manufacturer's instructions:

anti-Bcl2, B46620 (Transduction laboratories, Lexington, KY);

anti-Bcl-X$_L$, B22620 (Transduction laboratories, Lexington, KY);

anti-Mcl1, M54020 (Transduction laboratories, Lexington, KY);

anti-Bax, 13401A (Pharmingen, San Diego, CA) and

anti-Bad, B31420 (Transduction laboratories, Lexington, KY).

RESULTS

Genetic interaction between *Mel18* and *Bmi1* mutants

To further characterize the genetic and functional interactions between *Mel18* and *Bmi1*, *Mel18*$^{+/-}$;*Bmi1*$^{+/-}$ mice were intercrossed. *Mel18*$^{+/-}$;*Bmi1*$^{+/-}$ mice were externally normal and fertile but lacked their 13th ribs, suggesting subtle posterior transformations of the axial skeleton (H. K., unpublished). As shown in Table 1, *Mel18*$^{-/-}$;*Bmi1*$^{-/-}$,

Table 1. Offspring of intercrosses between compound heterozygous *Mel18* and *Bmi1* mutant mice

Genotype	Age				
	9.5 dpc	10.5 dpc	13.5 dpc	Newborn	Expected (%)
Mel18$^{+/+}$; *Bmi1*$^{+/+}$	6.9 (5)	13 (3)	5.6 (3)	12 (8)	6.3
Mel18$^{+/-}$; *Bmi1*$^{+/+}$	13 (9)	4.3 (1)	9.3 (5)	13 (9)	13
Mel18$^{+/+}$; *Bmi1*$^{+/-}$	19 (14)	13 (3)	13 (7)	33 (23)	13
Mel18$^{+/-}$; *Bmi1*$^{+/-}$	25 (18)	17 (4)	37 (20)	25 (17)	25
Mel18$^{-/-}$; *Bmi1*$^{+/+}$	6.9 (5)	4.3 (1)	1.9 (1)	7.2 (5)	6.3
Mel18$^{+/+}$; *Bmi1*$^{-/-}$	6.9 (5)	0 (0)	9.2 (5)	5.8 (4)	6.3
Mel18$^{-/-}$; *Bmi1*$^{+/-}$	2.8 (2)	26 (6)	19 (10)	1.4 (1*)	13
Mel18$^{+/-}$; *Bmi1*$^{-/-}$	9.7 (7)	22 (5)	5.6 (3)	2.9 (2*)	13
Mel18$^{-/-}$; *Bmi1*$^{-/-}$	9.7 (7)	0 (0)	0 (0)	0 (0)	6.3
	n=72	*n*=23	*n*=54	*n*=69	

*The number of dead pups are shown in parentheses.

Mel18$^{+/-}$;*Bmi-1*$^{-/-}$ and *Mel18*$^{-/-}$;*Bmi1*$^{+/-}$ mice did not survive until birth, whereas *Mel18*$^{-/-}$;*Bmi1*$^{+/+}$ or *Mel18*$^{+/+}$;*Bmi1*$^{-/-}$ pups did. *Mel18*$^{-/-}$;*Bmi1*$^{-/-}$ embryos survived until 9.5 dpc, whereas *Mel18*$^{+/-}$;*Bmi1*$^{-/-}$ and *Mel18*$^{-/-}$;*Bmi1*$^{+/-}$ fetuses survived significantly longer, some until the perinatal period. Thus, *Mel18* and *Bmi1* are required for the survival of embryos in a gene dose-dependent manner.

Similarly, malformations in the axial and appendicular skeletons increased in severity with a decrease in the *Mel18* and *Bmi1* gene dose (Fig. 1A). Thus, in the skull, cleft of the secondary palate was observed in all of *Mel18*$^{+/-}$;*Bmi1*$^{-/-}$ (6/6) and *Mel18*$^{-/-}$;*Bmi1*$^{+/-}$ (6/6) fetuses, whereas it was not seen in *Mel18*$^{-/-}$;*Bmi1*$^{+/+}$ (0/5) fetuses and was seen less frequently in *Mel18*$^{+/+}$;*Bmi1*$^{-/-}$ fetuses (2/6) (H. K., unpublished). The exoccipital bone was frequently split in *Mel18*$^{+/-}$;*Bmi1*$^{-/-}$ and *Mel18*$^{-/-}$;*Bmi1*$^{+/-}$ fetuses while such splitting was never seen in the single mutants (Fig. 1A). In the cervical region, the C1 vertebrae in single mutants exhibited mixed morphological properties of the atlas and axis, as is illustrated by the ossification center of anterior tuberculus and odontoid process. These structures were absent from the C1 vertebrae of *Mel18*$^{+/-}$;*Bmi1*$^{-/-}$ and *Mel18*$^{-/-}$;*Bmi1*$^{+/-}$ fetuses. Thus, the C1 vertebrae of *Mel18*$^{+/-}$;*Bmi1*$^{-/-}$ and *Mel18*$^{-/-}$;*Bmi1*$^{+/-}$ fetuses resembled C3 rather than C2 vertebrae of wild-type mice, indicative of stronger posterior transformations than seen in the single mutants (van der Lugt et al., 1994; Akasaka et al., 1996). In line with this, the anterior tuberculus of vertebral arteries normally present on the C6 vertebrae of the wild-type and single mutants were frequently observed on the C5 vertebrae of *Mel18*$^{+/-}$;*Bmi1*$^{-/-}$ and *Mel18*$^{-/-}$;*Bmi1*$^{+/-}$ fetuses. In addition, rudimentary ribs were attached to the C6 vertebrae in *Mel18*$^{+/-}$;*Bmi1*$^{-/-}$ and *Mel18*$^{-/-}$;*Bmi1*$^{+/-}$ fetuses but to C7 in the single mutants. In the rib cage, ribs attached to the C7 vertebrae frequently were alternately attached to the sternum in *Mel18*$^{+/-}$;*Bmi1*$^{-/-}$ and *Mel18*$^{-/-}$;*Bmi1*$^{+/-}$ fetuses. Furthermore, ectopic ossification centers were seen in the sternum of *Mel18*$^{+/-}$;*Bmi1*$^{-/-}$ and *Mel18*$^{-/-}$;*Bmi1*$^{+/-}$ fetuses. Taken together, these results indicate that the posterior transformations of the axial skeleton and rib cage were more complete and stronger in *Mel18*$^{+/-}$;*Bmi1*$^{-/-}$ and *Mel18*$^{-/-}$;*Bmi1*$^{+/-}$ fetuses than in the single mutants (Fig. 1B). Scapulae were also affected in a gene dose-dependent manner: acromion formation was strongly impaired and holes appeared in the center of the shoulder blades in *Mel18*$^{+/-}$;*Bmi1*$^{-/-}$ and *Mel18*$^{-/-}$;*Bmi1*$^{+/-}$ fetuses, which was not observed in the single mutants. Interestingly, defects of scapulae seen in *Mel18*$^{+/-}$;*Bmi1*$^{-/-}$ and *Mel18*$^{-/-}$;*Bmi1*$^{+/-}$ fetuses were reminiscent of shoulder blade defects observed in mice that lack *M33* (*Cbx2* – Mouse Genome Informatics; Coré et al., 1997).

To validate whether these defects were accompanied with changes in Hox gene expression boundaries, *Hoxb3* expression patterns in *Mel18*$^{-/-}$;*Bmi1*$^{+/-}$ and *Mel18*$^{+/-}$;*Bmi1*$^{-/-}$ embryos were compared with that in single mutants (Fig. 1C). Expression of *Hoxb3* was not observed in the neural crest-derived cells anterior to the otic vesicle in wild-type or single mutant embryos. In contrast, in *Mel18*$^{-/-}$;*Bmi1*$^{+/-}$ embryos, the expression of *Hoxb3* was seen in neural crest-derived cells migrating into the second branchial arches as indicated by an arrow. In *Mel18*$^{+/-}$;*Bmi1*$^{-/-}$ embryos, ectopic expression of *Hoxb3* was observed in mesenchymal cells beneath the
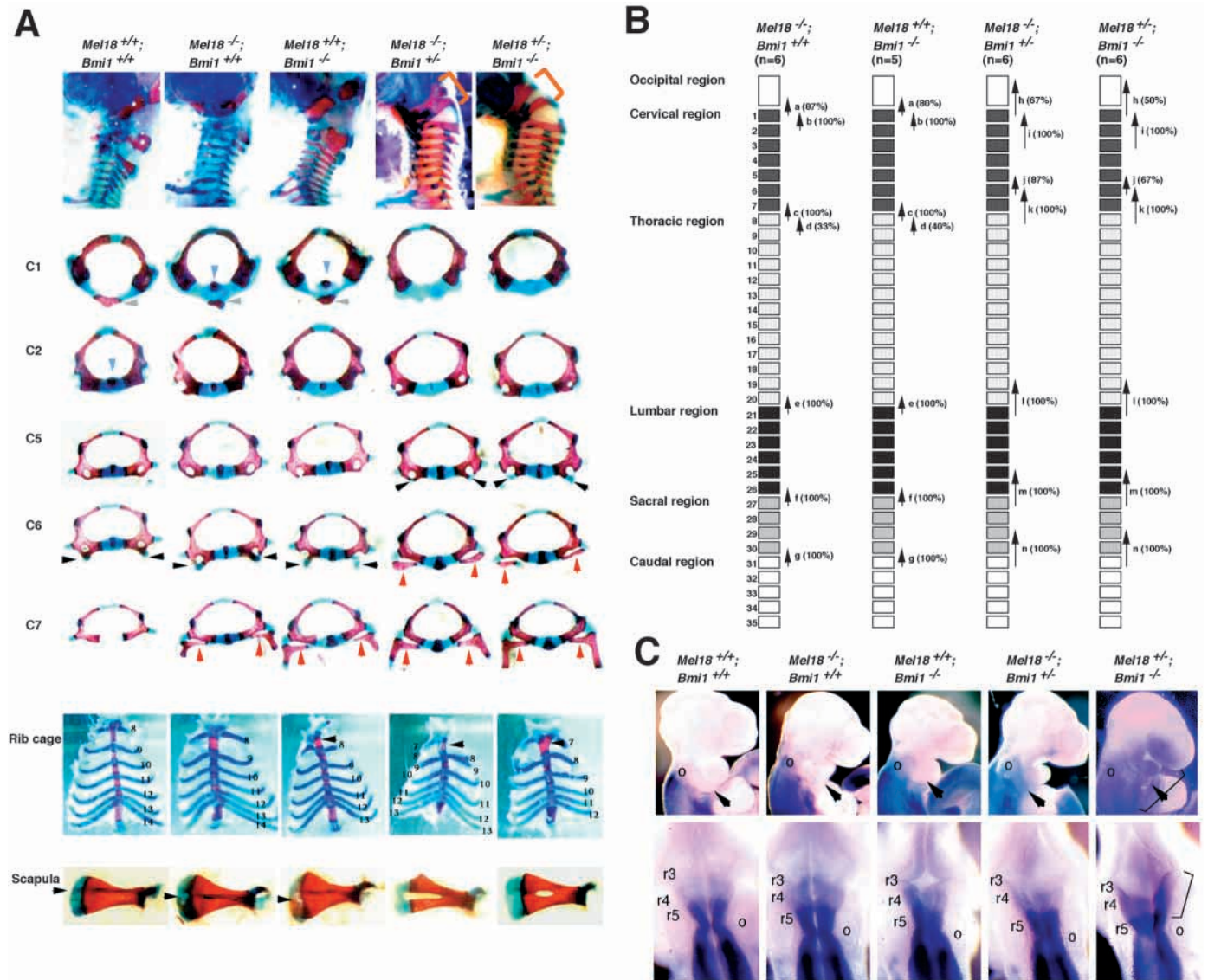
Fig. 1. Gene dose-dependent alterations of the axial and appendicular skeletons and *Hoxb3* gene expression in 9.5 dpc embryos. (A) Lateral views of occipitocervical region of the axial skeleton, overviews of individual C1, C2, C5, C6 and C7 vertebrae, ventral views of rib cages and overviews of scapulas are shown. In the lateral views of *Mel18⁻/⁻;Bmi1⁺/⁻* and *Mel18⁺/⁻;Bmi1⁻/⁻* vertebral columns, segmentation of exoccipital bones are indicated by brackets. In C1 and C2 vertebrae, anterior tuberculus and odontoid processes are indicated by grey and light-blue arrowheads, respectively. In C5 and C6 vertebrae, anterior tuberculus of vertebral arteries are indicated by black arrowheads. In C6 and C7 vertebrae, ectopic ribs are indicated by red arrowheads. In ventral views of rib cages, numbers of vertebrae to which ribs were attached are indicated. C1 vertebrae are counted as first vertebrae. In the scapula, note that the absence of acromion and generation of holes in the center of blades in *Mel18⁺/⁻;Bmi1⁻/⁻* and *Mel18⁻/⁻;Bmi1⁺/⁻* mice. Acromions are indicated by arrowheads. (B) Posterior transformations of the axial skeleton observed in of *Mel18⁻/⁻;Bmi1⁺/⁺*, *Mel18⁺/⁺;Bmi1⁻/⁻*, *Mel18⁻/⁻;Bmi1⁺/⁻* and *Mel18⁺/⁻;Bmi1⁻/⁻* mice are summarized. The following parameters were scored and frequency of each alteration are indicated in parentheses: (a) Supraoccipital bone→C1, appearance of the ectopic bones seen in the craniodorsal region of the C1 vertebra; (b) C1→C2, presence of the odontoid process on the C1 vertebra; (c) C7→T1, appearance of cervical ribs on C7; (d) T1→T2, prominent spinous process on T1; (e) T13→L1, loss of the rib in 20th vertebra; (f) L6→S1, formation of the sacro-iliac joint in 26th vertebra; (g) S4→Ca1, appearance of the first caudal vertebra in 30th vertebra, (h) Occipital bones→C1, segmentation of exoccipital bone; (i) C1→C3, miss of odontoid process in C1 and C2 vertebrae; (j) C4→C5, appearance of the anterior tubercle of the transverse process on the C5 vertebra, (k) C6→T1, appearance of cervical ribs on C6; (l) T12→L1, loss of the rib in 19th vertebra; (m) L5→S1, formation of the sacro-iliac joint in 25th vertebra; and (n) S3→Ca1, appearance of the first caudal vertebra in 29th vertebra. (C) The expression of *Hoxb3* in 9.5 dpc *Mel18⁺/⁺;Bmi1⁺/⁺*, *Mel18⁻/⁻;Bmi1⁺/⁺*, *Mel18⁺/⁺;Bmi1⁻/⁻*, *Mel18⁻/⁻;Bmi1⁺/⁻* and *Mel18⁺/⁻;Bmi1⁻/⁻* embryos. Lateral (upper) and dorsal (lower) views are shown. Ectopic expression of *Hoxb3* in mesenchymal cells beneath the optic vesicle (o) and in the first and second branchial arches in a *Mel18⁻/⁻;Bmi1⁺/⁻* embryo and in neural crest-derived cells migrating into the first and second branchial arches in a *Mel18⁻/⁻;Bmi1⁺/⁻* embryo are indicated by brackets. Arrowheads indicate second branchial arches.

optic vesicle and in the first and second branchial arches as indicated by parenthesis (Fig. 1C). These gene dose-dependent

alterations of *Hoxb3* expression in the neural crest-derived cells were observed in two out of three *Mel-18⁻/⁻;Bmi-1⁺/⁻* embryos
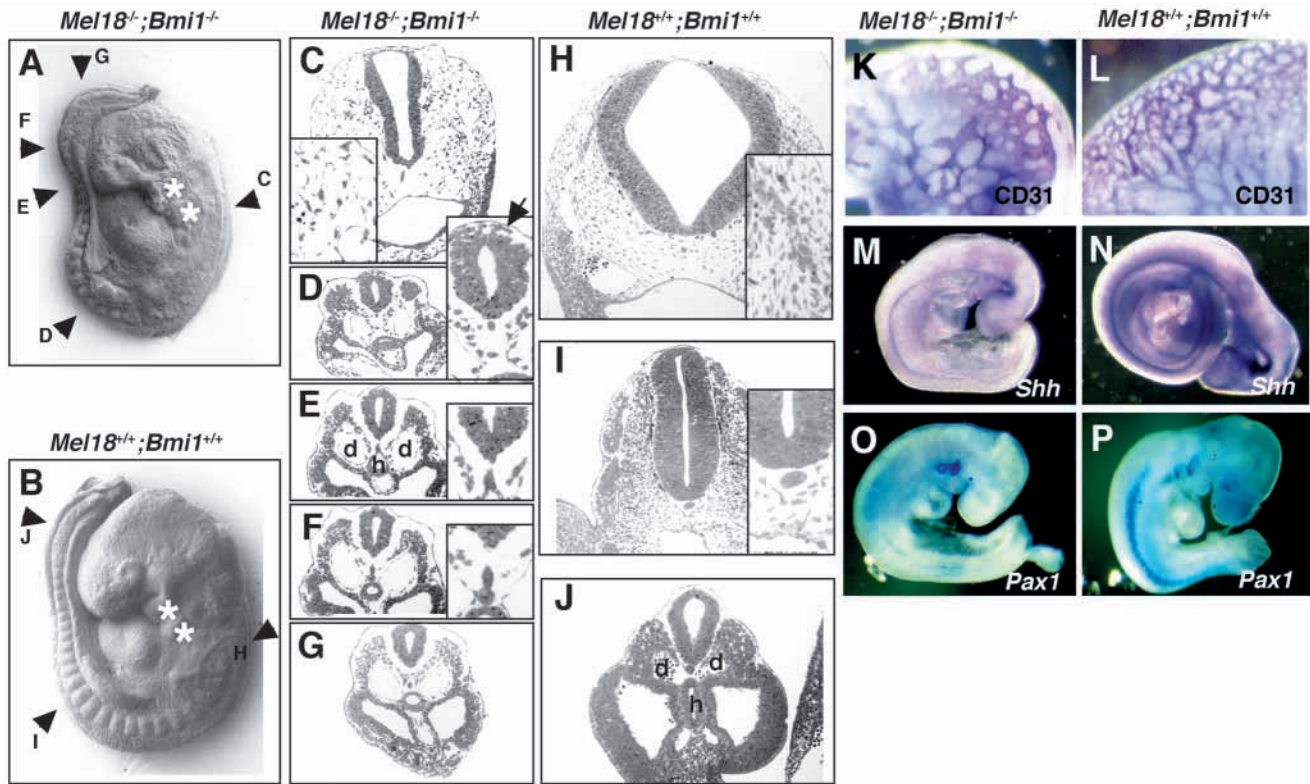
Fig. 2. Morphological alterations and the significant increase in apoptotic cells in 9.5 dpc $Mel18^{-/-};Bmi1^{-/-}$ embryos. (A) Scanning electron microscopic view of a 9.5 dpc $Mel18^{-/-};Bmi1^{-/-}$ embryo is shown. The second and third bronchial arches are indicated by asterisks. The levels of the transverse sections shown in C-G are indicated by arrowheads. (B) Scanning electron microscopic view of a 9.5 dpc wild-type embryo is shown. The second and third bronchial arches are indicated by asterisks. The levels of the transverse sections shown in H-J are indicated by arrowheads. (C) Transverse section of a 9.5 dpc $Mel18^{-/-};Bmi1^{-/-}$ embryo at the level of the hindbrain. (Inset) A higher magnification view of the paraxial mesoderm. Note that the fibroblastic cells are reduced and vascular endothelial cells are relatively increased. (D) Transverse section of a 9.5 dpc $Mel18^{-/-};Bmi1^{-/-}$ embryo at the level of prospective forelimb buds. Note that dorsal aorta failed to fuse at the midline and somitic mesoderm was not clearly differentiated into epithelial dermomyotome and mesenchymal sclerotome. (Inset) Higher magnification of the neural tube and notochord, and generation of neural crest cells in the dorsal region of the neural tube is indicated by an arrow. (E) Transverse section of a 9.5 dpc $Mel18^{-/-};Bmi1^{-/-}$ embryo at the level of newly segmented somite. Dorsal aorta (d) and hindgut (h) are indicated. (Inset) Higher magnification view of the ventral neural tube and notochord. Note that the notochord is fused with the hindgut. (F) Transverse section of a 9.5 dpc $Mel18^{-/-};Bmi1^{-/-}$ embryo at the level of cranial region of unsegmented paraxial mesoderm. (Inset) Higher magnification view of the ventral neural tube and notochord. Note that the notochord is bifurcated dorsoventrally. (G) Transverse section of a 9.5 dpc $Mel18^{-/-};Bmi1^{-/-}$ embryo at the level of caudal region of unsegmented paraxial mesoderm. (H) Transverse section of a 9.5 dpc wild-type embryo at the level of hindbrain. (Inset) Higher magnification view of the paraxial mesoderm. (I) Transverse section of a 9.5 dpc wild-type embryo at the level of prospective forelimb bud. Note that somitic mesoderm was clearly differentiated into epithelial dermomyotome and mesenchymal sclerotome. (Inset) Higher magnification view of the ventral neural tube and notochord. (J) Transverse section of a 9.5 dpc wild-type embryo at the level of cranial region of unsegmented paraxial mesoderm. Dorsal aorta (d) and hindgut (h) are indicated. Note that dorsal aorta is already fused. (K,L) The expression CD31, a vascular endothelial cell marker, in the cephalic region of 9.5 dpc $Mel18^{-/-};Bmi1^{-/-}$ (K) and wild-type (L) embryos. Note the expansion of sinus compared with the wild type. (L) The expression CD31, a vascular endothelial cell marker, in the cephalic region of 9.5 dpc wild-type embryo. (M,N) The expression of Shh in a 9.5 dpc $Mel18^{-/-};Bmi1^{-/-}$ embryo (M) was significantly reduced compared with the wild-type embryo (N). (O,P) Sclerotomal expression of $Pax1$ in a 9.5 dpc $Mel18^{-/-};Bmi1^{-/-}$ embryo (O) is significantly reduced compared with the wild-type embryo (P), while the expression in the pharyngeal pouches was not affected. (P) The expression of $Pax1$ in a 9.5 dpc wild-type embryo is shown.

and two out of four $Mel\text{-}18^{+/-};Bmi\text{-}1^{-/-}$ embryos. This is in good agreement with mild variations in penetrance of skeletal alterations seen between individual $Mel\text{-}18^{+/-};Bmi\text{-}1^{-/-}$ and $Mel\text{-}18^{-/-};Bmi\text{-}1^{+/-}$ fetuses, as was also observed previously for the single mutants (van der Lugt et al., 1994; Akasaka et al., 1996). The expression of $Hoxb3$ in the neural tube was affected in less extent. In single mutant and $Mel18^{-/-};Bmi1^{+/-}$ embryos, slight de-repression was seen in the rhombomere 4 (r4). In two out of four $Mel18^{+/-};Bmi1^{-/-}$ embryos, $Hoxb3$ was strongly expressed in r4 as indicated by the parenthesis. Thus,

the de-repression of $Hoxb3$ expression in the cranial and branchial neural crest cells was suggested to occur during the migration of the neural crest cells as observed in $rae28/Mph1$-deficient mice (Takihara et al., 1997).

## Growth of embryonic tissues is affected in $Mel18^{-/-};Bmi1^{-/-}$ embryos

$Mel18^{-/-};Bmi1^{-/-}$ embryos developed normally up to 8.5 dpc, but severe growth retardation and abnormalities were evident in 9.5 dpc embryos, although survival of these embryos was

confirmed by visual inspection of a heart beat at the time of dissection. Scanning electron microscopic analysis of 9.5 dpc embryos revealed that on average approximately 18 somites were generated in $Mel18^{-/-};Bmi1^{-/-}$ embryos, whereas more than 24 somites were formed in $Mel18^{+/+};Bmi1^{+/+}$, $Mel18^{-/-};Bmi1^{+/+}$, $Mel18^{+/+};Bmi1^{-/-}$ and $Mel18^{-/-};Bmi1^{+/-}$ littermates (Fig. 2A,B; T. A. and H. K., unpublished). At this stage, $Mel18^{-/-};Bmi1^{+/-}$ and $Mel18^{+/-};Bmi1^{-/-}$ embryos were externally indistinguishable from wild-type embryos (T. A. and H. K., unpublished). In the cranial region, the first and second branchial arches were poorly developed and the optic eminence was obscure in $Mel18^{-/-};Bmi1^{-/-}$ embryos. Somitic mesoderm in the presumptive trunk region was segmented at the appropriate position however the somites were not aligned regularly (compare Fig. 2A with Fig. 2B). In the caudal region, the distal tip of the tail bud was significantly shrunken in $Mel18^{-/-};Bmi1^{-/-}$ embryos (Fig. 2A). The specific morphological alterations seen in $Mel18^{-/-};Bmi1^{-/-}$ embryos with 18 somites were not observed in wild-type and single mutant embryos of 18 somite stages, indicating that defects in $Mel18^{-/-};Bmi1^{-/-}$ embryos were not due to indirect consequences of an overall growth retardation.

Transverse sections revealed severe morphological abnormalities in the neural tube, paraxial mesoderm and notochord of $Mel18^{-/-};Bmi1^{-/-}$ embryos that were not seen in the single mutants (Fig. 2). At the level of the heart primordium, the hindbrain was clearly less developed compared with wild-type or single mutants and many pyknotic

figures were observed. In the paraxial mesoderm, the density of the mesenchymal cells was significantly reduced and endothelial cells were relatively increased in number in $Mel18^{-/-};Bmi1^{-/-}$ embryos (Fig. 2C,H). The expression of CD31, an endothelial cell marker, also indicated the extensive dilatation of blood vessels in the cranial region of $Mel18^{-/-};Bmi1^{-/-}$ embryos (Fig. 2K,L). At the level of the forelimb buds, the neural tube, the notochord and somitic mesoderm were reduced in size in $Mel18^{-/-};Bmi1^{-/-}$ embryos in comparison with wild type or single mutants (Fig. 2D-F,I). Generation of the neural crest cells was visible whereas de-epithelization of somites and fusion of the dorsal aorta at the midline were clearly impaired (Fig. 2D,I). Both neuronal and mesodermal cell numbers were reduced in the caudal region, whereas the dorsal aorta was relatively expanded in $Mel18^{-/-};Bmi1^{-/-}$ embryos (Fig. 2E). The integrity of the notochord was strongly affected, as evidenced by reduction in size, bifurcation and fusion with the hindgut endoderm in $Mel18^{-/-};Bmi1^{-/-}$embryos (Fig. 2D-G,I,J). This observation attempted us to investigate the expression of sonic hedgehog (Shh), a functional marker of the notochord. Shh expression in the notochord was significantly reduced in $Mel18^{-/-};Bmi1^{-/-}$ embryos, suggesting functional impairment of the notochord (Fig. 2M,N). Concordantly, Shh-dependent expression of $Pax1$ in the somitic mesoderm (Fan and Tessier-Lavigne, 1994) was reduced, although the expression in pharyngeal pouch endoderm was not affected (Fig. 2O,P). Thus, the fact that maintenance but not initial generation of the notochord is

Fig. 3. Altered Hox gene expression in $Mel18^{-/-};Bmi1^{-/-}$ embryos. (A) Expression of $Hoxb6$ in a 9.5 dpc $Mel18^{-/-};Bmi1^{-/-}$ embryo. Note that the anterior boundary of $Hoxb3$ expression was shifted up to forebrain. (B) Expression of $Hoxb3$ in a 9.5 dpc wild-type embryo. (C) Expression of $Hoxb6$ in a 9.5 dpc $Mel18^{-/-};Bmi1^{-/-}$ embryo. Note that the anterior boundary of $Hoxb6$ expression was shifted up to forebrain. (D) Expression of $Hoxb6$ in a 9.5 dpc wild-type embryo. (E) Expression of $Hoxd4$ in a 9.5 dpc $Mel18^{-/-};Bmi1^{-/-}$ embryo. Note that original anterior boundary of $Hoxd4$ expression was still visible and the expression in the cranial region was not totally de-repressed. (F) Expression of $Hoxd4$ in a 9.5 dpc wild-type embryo. (G) Expression of $Hoxc6$ in a 9.5 dpc $Mel18^{-/-};Bmi1^{-/-}$ embryo. (H) Bright field view of G. (I) Expression of $Hoxc6$ in a 9.5 dpc wild-type embryo. (J) Bright field view of I. (K) The expression of $Hoxb6$ and $Hoxd13$ genes in the cranial region was examined by RT-PCR. Two individual $Mel18^{-/-};Bmi1^{-/-}$ embryos and a wild-type embryo were separated into cranial (cr) and trunk (tr) regions, as described in the text. β-Actin was used as a control. (L) The expression of $Hoxb6$ in an 8.5 dpc $Mel18^{-/-};Bmi1^{-/-}$ embryo. Note that $Hoxb6$ transcripts were restricted in the caudal region of the embryo. (M) The expression of $Hoxb6$ in an 8.5 dpc wild-type embryo.
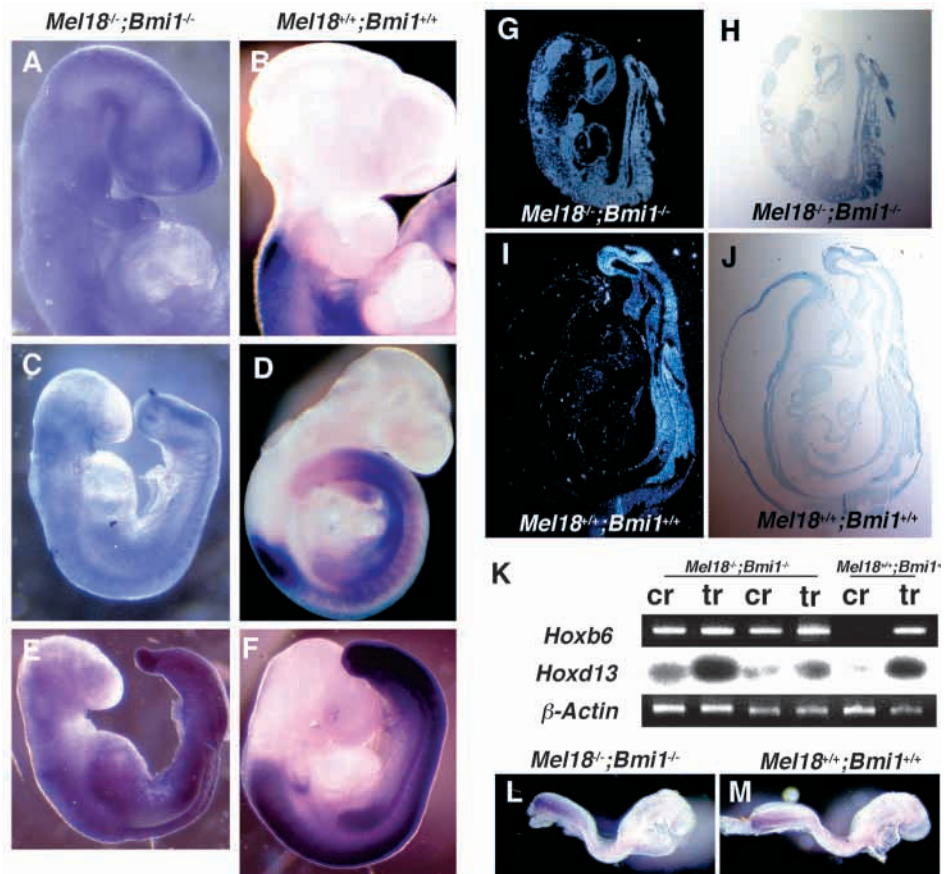
affected in *Mel18⁻/⁻;Bmi1⁻/⁻* embryos indicates that gastrulation per se is not dependent on the Mel18 and Bmi1 proteins. In contrast, exponential outgrowth of the neural tube and paraxial mesoderm does depend on the proper amount of Mel18 and Bmi1 proteins.

Maintenance but not establishment of Hox gene expression is affected in *Mel18⁻/⁻;Bmi1⁻/⁻* embryos

The expression of *Hoxb3, Hoxb6, Hoxd4* and *Hoxc6* was examined in 9.5 dpc *Mel18⁻/⁻;Bmi1⁻/⁻* embryos. *Hoxb3, Hoxb6* and *Hoxc6* expression was uniformly extended to the fore- or midbrain, while the expression in wild-type or single mutant embryos was restricted to the presumptive cervical region of the neural tube (Fig. 3A-D,G-J and T. A. and H. K., unpublished) (Akasaka et al., 1996; van der Lugt et al., 1996). *Hoxd4* expression was also extended anteriorly in double mutants while de-repression in the cranial region was less prominent compared to *Hoxb3, Hoxb6* and *Hoxc6* expression (Fig. 3E,F). To further confirm these observations, 9.5 dpc embryos were dissected into three pieces at the level of midbrain/hindbrain boundary and forelimb bud, and the expression of *Hoxb6* in the cranial and caudal region was investigated by semi-quantitative RT-PCR. Ectopic expression of *Hoxb6* in the fore- or midbrain was again demonstrated (Fig. 3K). Therefore, the anterior expression boundaries of *Hoxb6* are substantially shifted in the anterior direction in *Mel18⁻/⁻;Bmi1⁻/⁻* embryos, while the shifts in single mutants are subtle. In sharp contrast, the expression boundary of *Hoxb6* in 8.5 dpc *Mel18⁻/⁻;Bmi1⁻/⁻* embryos was normally localized in the caudal region (compare doubly mutant Fig. 3L with wild type Fig. 3M), which is in line with the absence of evident morphological alterations at this stage. The expression of *Hoxd13*, which is expressed up to the presumptive sacrocaudal boundary, was also investigated because its expression domain is first observed at 9.5 dpc (Dollé et al., 1991). *Hoxd13* expression turned out not to be significantly de-repressed in the cranial region of 9.5 dpc *Mel18⁻/⁻;Bmi1⁻/⁻* embryos (Fig. 3K). Together, these results indicate that the initial establishment of the anterior boundaries of Hox cluster genes is not dependent upon Mel18 and Bmi1, while the stable maintenance of repression of Hox genes in the anterior region is essentially dependent on the Mel18 and Bmi1 gene products.

Interestingly, in addition to the ectopic expression (de-repression) of Hox genes in *Mel18⁻/⁻;Bmi1⁻/⁻* embryos, a significant overall reduction of *Hoxb6* expression in the presumptive trunk region was revealed by quantitative RT-PCR (Fig. 4) and in situ hybridization (Fig. 3C). *Hoxb6* expression in the trunk region of *Mel18⁻/⁻;Bmi1⁻/⁻* embryos was estimated to be approximately one quarter of that of wild-type embryos. We further examined the expression of *Evx1* which localizes at the 5′ end of the *Hoxa* cluster. *Evx1* expression, indeed, was significantly downregulated in *Mel18⁻/⁻;Bmi1⁻/⁻* embryos, compared to the wild-type and single mutant embryos (Fig. 5). Therefore, in apparent contrast to their well-documented action in repressive PcG complexes, Mel18 and Bmi1 are also required to maintain the transcription of Hox cluster genes and neighboring *Evx1* gene in the posterior region.

Accelerated apoptosis in *Mel18⁻/⁻;Bmi1⁻/⁻* embryos

Transmitting electron microscopic analysis of the developing neural tube indicated that morphological alterations

characteristic for cells undergoing apoptosis (Kerr et al., 1995) were frequently seen in *Mel18⁻/⁻;Bmi1⁻/⁻* embryos (Fig. 6A,B). Cell-to-cell adhesion of neural tube cells was impaired and extensive protrusion or blebbing of the cell surface was observed in *Mel-18⁻/⁻;Bmi-1⁻/⁻* embryos. Extensive vacuoles in the cytoplasm and apoptotic bodies were also frequently seen (Fig. 6A, arrows). Within the nucleus, the chromatin was hypercondensed in the doubly deficient embryos. The same alterations were observed in the notochord, paraxial mesoderm, lateral plate mesoderm and hindgut (T. A. and H. K., unpublished). TUNEL staining also demonstrated significant acceleration of apoptosis in the cranial and presumptive trunk regions of *Mel18⁻/⁻;Bmi1⁻/⁻* embryos (Fig. 6C-F). Apoptotic cells were present ubiquitously at this stage, although they were not predominantly seen in 8.5 dpc doubly deficient embryos (T. A. and H. K., unpublished).
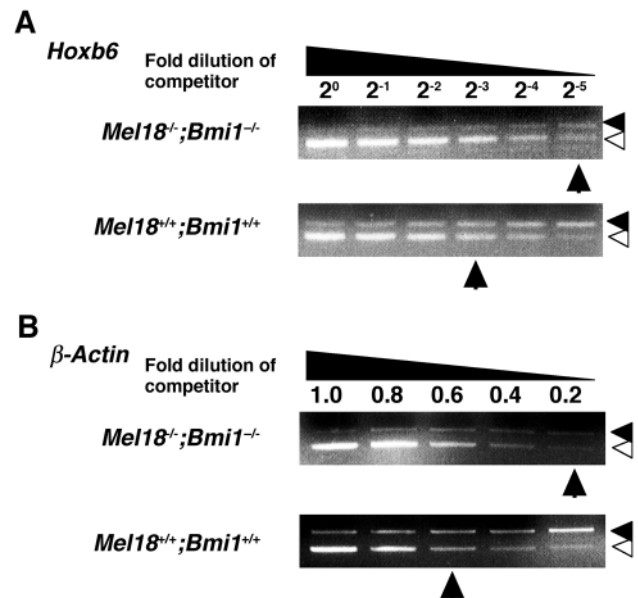

Fig. 4. Relative amount of *Hoxb6* expression in the trunk region was compared between *Mel18⁻/⁻;Bmi1⁻/⁻* and wild-type embryos by competitive RT-PCR. (A) The expression of *Hoxb6*. Briefly, serially diluted amounts of competitor DNA were amplified with the fixed amount of cDNA synthesized from total cellular RNA extracted from *Mel18⁻/⁻;Bmi1⁻/⁻* or wild-type embryos. PCR products derived from the cellular cDNA and the competitor DNA are indicated by closed and open arrowheads, respectively. In the wild type, PCR products from cellular RNA and competitor DNA were balanced in 2^{-3} dilution while 2^{-5} dilution in *Mel18⁻/⁻;Bmi1⁻/⁻* as indicated by vertical arrowheads. It implies that *Hoxb6* expression in *Mel18⁻/⁻;Bmi1⁻/⁻* embryos is reduced to 25% of that in the wild type. (B) The expression of the gene for β-actin for standardization of amounts of cDNA between *Mel18⁻/⁻;Bmi1⁻/⁻* and wild-type embryos. PCR products derived from the cellular cDNA and the competitor DNA are indicated by black and white arrowheads, respectively. In the wild type, PCR products from cellular RNA and competitor DNA were balanced at 0.6-fold dilution, whereas in *Mel18⁻/⁻;Bmi1⁻/⁻* mice, they were balanced at 0.2-fold dilution, as indicated by vertical arrowheads. Thus, three times volume of cDNA synthesized from *Mel18⁻/⁻;Bmi1⁻/⁻* embryonic RNA compared with that from the wild type was subjected to PCR reaction for *Hoxb6* expression.
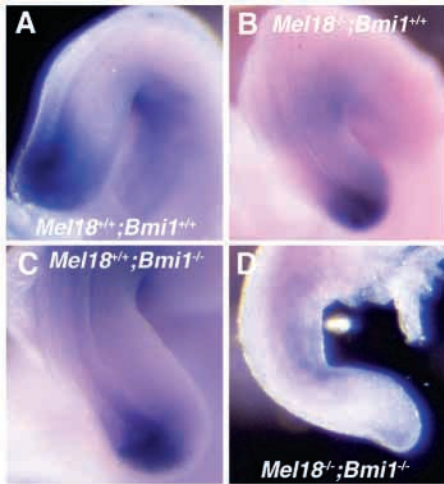
Fig. 5. The expression of *Evx1* in the wild type (A), *Mel18⁻/⁻;Bmi1⁺/⁺* (B), *Mel18⁺/⁺;Bmi1⁻/⁻* (C) and *Mel18⁻/⁻;Bmi1⁻/⁻* (D) embryos. Tail buds of 9.5 dpc embryos are shown.

In *Bmi1⁻/⁻* thymocytes, increased apoptosis was shown to be due at least in part by upregulation of the tumor suppressor p19^{Arf} (Jacobs et al., 1999a). This prompted us to look at the expression of *p19^{Arf}* and *p16* (Cdkn2a – Mouse Genome Informatics) in 9.5 dpc doubly deficient embryos. Semi-quantitative RT-PCR analyses revealed about at least 10 fold up-regulation of *p19^{Arf}* and *p16* expression (Fig. 6G). Thus, significant upregulation of p19^{Arf} could in part be causative for accelerated apoptosis in *Mel18⁻/⁻;Bmi1⁻/⁻* embryos. We further investigated the expression of Bcl2 family gene products, which function as pro-survival or pro-apoptotic proteins under diverse cytotoxic insults, because overexpression of *Bcl2* gene product significantly restored the number of thymocytes in *Bmi1*-deficient mice and the expression of Bad protein, an agonist of cell death, was significantly increased in thymocytes of *Mel18* single mutant mice, whereas no such increase of Bad was seen in *Bmi1⁻/⁻* thymocytes (M. K., unpublished). The level of the Bad protein was significantly increased while other Bcl2 family gene products examined were unaffected in *Mel18⁻/⁻;Bmi1⁻/⁻* embryos (Fig. 6H) (M. K., unpublished). These results are consistent with the above-described observations, which

Fig. 6. Accelerated apoptosis in *Mel18⁻/⁻;Bmi1⁻/⁻* embryos is accompanied with overexpression of *Bad* gene product.
(A,B) Transmitting electron microscopic view of the neural tube of a 9.5 dpc *Mel18⁻/⁻;Bmi1⁻/⁻* embryo (A) and wild-type embryo (B) is shown. Apoptotic bodies are indicated by arrows. These are adjacent sections to those in Fig. 2.
(C,D) Apoptotic cells in the cranial region of a 9.5 dpc *Mel18⁻/⁻;Bmi1⁻/⁻* (C) and wild-type (D) embryos are shown by using TUNEL staining.
(E,F) Apoptotic cells in the trunk region of a 9.5 dpc *Mel18⁻/⁻;Bmi1⁻/⁻* (E) and wild-type (F) embryos are shown by using TUNEL staining. (G) The expression of p19^{Arf} and p16^{ink4a} is compared between the wild-type and *Mel18⁻/⁻;Bmi1⁻/⁻* 9.5 dpc embryos. Prior to semi-quantitative RT-PCR analyses, the total amount of cDNA is normalized by competitive RT-PCR for β-actin expression. Varied amounts of competitor DNA (black horizontal arrowheads), were amplified in the same tube with embryonic cDNA (white horizontal arrowheads). The amount of cDNA indicated by vertical arrowheads is used for analyses. (H) The expression of Bcl2 family proteins including Bcl2, Bcl-X$_L$, Mcl1, Bax and Bad

are revealed by western blot analysis. Note the overexpression of Bad protein while other gene products unaffected in 9.5 dpc *Mel18⁻/⁻;Bmi1⁻/⁻* embryos. (I) The expression of mRNA encoding Bcl2 family proteins including Bcl2, Bcl-X$_L$, Bax and Bad are revealed by RT-PCR. Note the expression of *Bad* is not significantly affected in 9.5dpc *Mel18⁻/⁻;Bmi1⁻/⁻* embryos compared with the wild type.
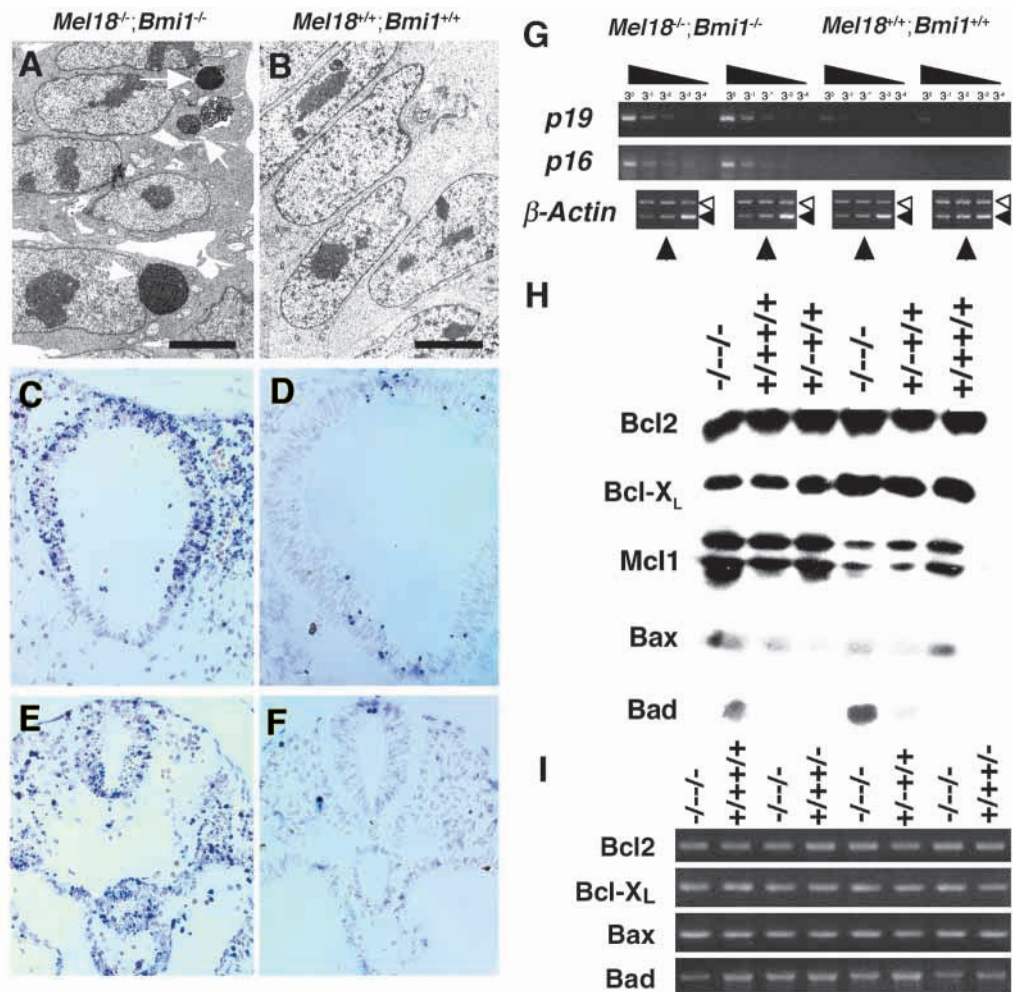
are indicative of significantly accelerated apoptosis in *Mel18*^{−/−}*;Bmi1*^{−/−} embryos. Despite the increase in protein levels, the mRNA expression of the *Bad* gene was not affected in *Mel18*^{−/−}*;Bmi1*^{−/−} embryos (Fig. 6I). Thus, overexpression of Bad protein in *Mel18*^{−/−}*;Bmi1*^{−/−} embryos might be due to indirect effects on the stability of Bad protein or translational control.

DISCUSSION

In this study, we have shown that compound *Mel18/Bmi1*-deficient mice reveal a strong exacerbation of the phenotypes of *Bmi1* or *Mel18* single mutant mice. Foremost, this is evident from the significant shortened life span of the doubly deficient embryos, which die around 9.5 dpc displaying severe growth retardation and abnormalities in somite alignment, neural tube, paraxial mesoderm and notochord morphology. This is in sharp contrast to the single mutant mice, which are born without these severe malformations. Furthermore, *Mel18*^{+/−}*;Bmi1*^{−/−} and *Mel18*^{−/−}*;Bmi1*^{+/−} newborn mice show a more pronounced and complete posterior transformations of the axial and appendicular skeleton than those seen in mice that lack either Bmi1 or Mel18, or even in *M33*^{−/−}*;Bmi1*^{−/−} doubly deficient mice (van der Lugt et al., 1994; Akasaka et al., 1996; Bel et al., 1998). The severe morphological abnormalities and posterior transformations are accompanied with pronounced anterior shifts in Hox gene expression boundaries (Fig. 3). These findings are in line with the ability of the highly related Mel18 and Bmi1 proteins to regulate largely overlapping sets of Hox target genes (Akasaka et al., 1996; van der Lugt et al., 1996). In addition to their effects on Hox gene expression, we show that Bmi1 and Mel18 are both required to regulate other target genes. This is well illustrated by the dramatically enhanced apoptosis in doubly deficient embryos. Thus, both genetic and biochemical evidence favor the conclusion that Bmi1 and Mel18 act in the same PcG complex, which most probably represents the mammalian ortholog of the recently described *Drosophila* PRC1 complex (Shao et al., 1999). This is further supported by the observation of characteristic scapulae defects in *Mel18*^{+/−}*;Bmi1*^{−/−} and *Mel18*^{−/−}*;Bmi1*^{+/−} mice. These defects are not present in single *Mel18*- or *Bmi1*-deficient mice, but are found in mice deficient for another mammalian 'PRC1' complex member, M33/Cbx2 (Coré et al., 1997). Together, these results clearly indicate a strict dose-dependent requirement for both Mel18 and Bmi1 in regulating proper repression of Hox and other target genes.

Next to the 'PRC1' type PcG complex, a separate mammalian protein complex has recently been described that harbors the PcG proteins Eed, Enx1 and Enx2, as well as several HDACs (Histone decateylases) (Sewalt et al., 1998; van der Vlag and Otte, 1999; van Lohuizen et al., 1998). Interestingly, *eed*-deficient mice die during mid-gastrulation (5-6 dpc), before the first onset of Hox gene expression, with defective embryonic mesoderm formation (Schumacher et al., 1996). This evidently represents an earlier and more severe embryonic defect than is observed in the *Mel18;Bmi1* doubly deficient embryos, which proceed through gastrulation, form embryonic mesoderm and initiate organ formation, but die around the 18 somite stage (9.5 dpc). Importantly, the pendant of the Eed/Enx complex in *Drosophila* has been shown to be required for initiation but not subsequent maintenance of Hox gene repression (Gutjahr et al., 1995; Jones et al., 1998; Ng et al., 2000; Simon et al., 1995; Struhl and Brower, 1982; Tie et al., 1998). Although there is currently no direct evidence, it is tempting to speculate, based on the conservation of the respective PcG complexes and the analysis of mouse mutants, that the Eed/Enx complex may fulfill an analogous function in mice. Assuming this speculation is warranted, how can the differences in phenotypes between the *eed* mutant and *Mel18;Bmi1* doubly deficient embryos be explained? Two distinct hypotheses can be posed. Firstly, it is formally possible that the Mel18/Bmi1-containing complex and the Eed/Enx complex fulfill independent functions and regulate different sets of target genes. Support for this comes from studies of hemopoietic precursor cells. *Bmi1*- or *Mel18*-deficient mice show severe lymphoproliverative defects, which can at least in part can be attributed to de-repression of the *Ink4a/Arf* tumor suppressor genes. In contrast, mice partially deficient for *eed* show increased proliferation of hemopoietic precursors, probably because of changes in transcription of as yet undefined target genes (Jacobs et al., 1999a; Lessard et al., 1999). However, a counter argument is that mice harboring an *eed*-hypomorphic allele do display skeletal defects reminiscent of those found in *Mel18* or *Bmi1* single mutant mice (Schumacher et al., 1996), suggesting the different complexes may regulate overlapping sets of Hox genes. A second theoretical possibility is that, besides *Mel18* and *Bmi1*, a third related gene exists that can partially compensate for loss of *Mel18* and *Bmi1*. Mammalian homologs of *Drosophila Polycomb* set a precedent in this respect, as next to *M33/Cbx2* and *Mpc2*, a third related gene (*Mpc3*) has recently been found (Gunster et al., 1997; Hemenway et al., 2000). This could explain why even in the doubly deficient embryos still some Hox gene expression patterns, such as that of *Hoxd4* appear to be affected to a lesser extent (Fig. 3). If such a gene exists, it probably represents a more distant relative or is expressed during a narrow (early) time window during development, as it cannot efficiently complement the defects in either the single mutants or the *Mel18/Bmi1* doubly deficient embryos. The sequencing of the entire mouse genome will soon allow us to confirm or disprove the latter possibility.

Notwithstanding their high degree of similarity, their biochemical interactions with the same set of PcG proteins and their action on overlapping sets of Hox genes, loss of either *Mel18* or *Bmi1* also leads to unique phenotypes indicative of effects on separate target genes (Akasaka et al., 1996; van der Lugt et al., 1994). This is further illustrated (in this study) by the severely enhanced effects on apoptosis in *Mel18/Bmi1* doubly deficient mice. Although increased apoptosis in hemopoietic cells of newborn *Bmi1*-deficient mice has been attributed, at least in part, to the de-repression of the *p19*^{*Arf*} tumor suppressor gene through a p53-dependent mechanism (Jacobs et al., 1999b), increased apoptosis in *Mel18*-deficient mice appears to be associated instead with an increased levels of the pro-apoptotic Bad protein (M. K., unpublished). In contrast to *Mel18/Bmi1* doubly deficient mice, both single mutant mice proceed normally through early embryonic development, with no evidence of increased apoptosis. This strongly suggests that a synergistic effect of

both increased Bad protein levels combined with elevated levels of p19^{Arf}/p53-dependent apoptosis is responsible for apoptosis in the doubly deficient embryos. The mechanism that underlies the increased Bad protein levels remains to be elucidated, but evidently represent an indirect effect of loss of *Mel18*, as the effects are not due to increased *Bad* mRNA levels.

Mel18/Bmi1 deficient embryos display normal anterior expression boundaries of *Hoxb6* and *Hoxc6* at 8.5 dpc and show normal processing through gastrulation, notochord formation and initiation of somite formation and organogenesis. In contrast, severe anterior expression boundary shifts of *Hoxb6* and *Hoxc6* are seen, combined with the initiation of proliferative defects and morphological abnormalities, from 9.5 dpc onwards. Similarly, the ectopic expression of *Hoxb3* was more prominently observed in the migrating neural crest cells than in the neural tube of *Mel18*$^{-/-}$;*Bmi1*$^{+/-}$ and *Mel18*$^{+/-}$;*Bmi1*$^{-/-}$ embryos (Fig.1C). This implies that the de-repression of *Hoxb3* takes place during the migration of neural crest cells. Together, this clearly indicates a requirement for *Mel18* and *Bmi1* for maintenance, but not initiation, of correct Hox gene expression boundaries. This is similar to the observation in mice lacking the *Mll* Trithorax Group (TrxG) gene that the expression of *Hoxa7* is lost at 9.5 dpc, whereas up to 8.5 dpc is normal (Yu et al., 1998). Together, these data suggest a transition from an early induction phase of Hox gene expression to a later maintenance phase between 8.5 dpc and 9.5 dpc, and further suggest that the opposing functions of TrxG activators and PcG repressors are required to maintain correct boundaries of Hox gene expression.

Interestingly, we found *Hoxb6* expression to be affected not only spatially but also quantitatively in *Mel18/Bmi1* doubly deficient embryos (Fig. 4). Similarly, the expression of *Evx1*, which is localized in the close proximity of the *Hoxa* cluster, is significantly downregulated in 9.5 dpc *Mel18*$^{-/-}$;*Bmi1*$^{-/-}$ embryos (Fig. 5). This, at first, may seem surprising, given the fact that TrxG and PcG protein complexes are thought to act as antagonists. Moreover, PcG proteins so far have been described to mediate Hox gene repression, but to our knowledge have not been found to be required for maintenance of the actively transcribed state. However, in *Drosophila*, extensive co-localization of Polycomb-responsive elements (PREs) between certain PcG and TrxG proteins has recently been described on polytene chromosomes (Chinwalla et al., 1995; Orlando et al., 1998). By analogy, Mll protein is also overexpressed in mammalian cells and has been shown to exhibit extensive co-localization with endogenous Bmi1 protein (Hanson et al., 1999). Furthermore, several members of the TrxG group can be classified as activators in one context, but can act as repressors on other target genes (LaJeunesse and Shearn, 1996), and certain TrxG proteins, such as GAGA, can be found on repressed PREs. These results suggest that TrxG and PcG complexes act in close proximity and perhaps should be envisaged as one imprinting machinery (van Lohuizen, 1999). Accordingly, loss of Mel18 and Bmi1 may affect also certain TrxG functions. Alternatively, more indirect mechanisms can be envisaged, in which loss of Mel18 and Bmi1 may, for example, lead to de-repression of a transcriptional repressor of TrxG genes. Clearly, further experimentation is needed to discriminate between these possibilities.

In summary, our analysis of *Mel18/Bmi1* doubly deficient mice reveals a strong synergistic requirement for these PcG proteins in the maintenance but not the initiation of Hox gene expression, as well as the regulation of other target genes, such as those controlling cell survival during early development. In addition, our results reinforce the functional differences in between the biochemically distinct Eed/Enx- and Bmi1/Mel18-containing PcG complexes. Furthermore, we describe a striking requirement for Mel18 and Bmi1 in maintaining proper expression levels of specific Hox genes, supporting the view that TrxG and PcG complexes act in an integrated manner in the regulation of Hox genes.

REFERENCES

Akasaka, T., Kanno, M., Balling, R., Mieza, M. A., Taniguchi, M. and Koseki, H. (1996). A role for mel-18, a Polycomb group-related vertebrate gene, during theanteroposterior specification of the axial skeleton. *Development* **122**, 1513-1522.

Akasaka, T., Tsuji, K., Kawahira, H., Kanno, M., Harigaya, K., Hu, L., Ebihara, Y., Nakahata, T., Tetsu, O., Taniguchi, M. and Koseki, H. (1997). The role of mel-18, a mammalian Polycomb group gene, during IL-7- dependent proliferation of lymphocyte precursors. *Immunity* **7**, 135-146.

Alkema, M. J., Bronk, M., Verhoeven, E., Otte, A., van't Veer, L. J., Berns, A. and van Lohuizen, M. (1997). Identification of Bmi1-interacting proteins as constituents of a multimeric mammalian polycomb complex. *Genes Dev.* **11**, 226-240.

Bel, S., Coré, N., Djabali, M., Kieboom, K., Van der Lugt, N., Alkema, M. J. and Van Lohuizen, M. (1998). Genetic interactions and dosage effects of Polycomb group genes in mice. *Development* **125**, 3543-3551.

Chinwalla, V., Jane, E. P. and Harte, P. J. (1995). The Drosophila trithorax protein binds to specific chromosomal sites and is co-localized with Polycomb at many sites. *EMBO J* **14**, 2056-2065.

Coré, N., Bel, S., Gaunt, S. J., Aurrand-Lions, M., Pearce, J., Fisher, A. and Djabali, M. (1997). Altered cellular proliferation and mesoderm patterning in Polycomb-M33- deficient mice. *Development* **124**, 721-729.

Dollé, P., Izpisua-Belmonte, J. C., Boncinelli, E. and Duboule, D. (1991). The Hox-4.8 gene is localized at the 5′ extremity of the Hox-4 complex and is expressed in the most posterior parts of the body during development. *Mech. Dev.* **36**, 3-13.

Fan, C. M. and Tessier-Lavigne, M. (1994). Patterning of mammalian somites by surface ectoderm and notochord: evidence for sclerotome induction by a hedgehog homolog. *Cell* **79**, 1175-1186.

Franke, A., DeCamillis, M., Zink, D., Cheng, N., Brock, H. W. and Paro, R. (1992). Polycomb and polyhomeotic are constituents of a multimeric protein complex in chromatin of Drosophila melanogaster. *EMBO J* **11**, 2941-2950.

Gebuhr, T. C., Bultman, S. J. and Magnuson, T. (2000). Pc-G/trx-G and the SWI/SNF connection: developmental gene regulation through chromatin remodeling. *Genesis* **26**, 189-197.

Gunster, M. J., Satijn, D. P., Hamer, K. M., den Blaauwen, J. L., de Bruijn, D., Alkema, M. J., van Lohuizen, M., van Driel, R. and Otte, A. P. (1997). Identification and characterization of interactions between the vertebrate polycomb-group protein BMI1 and human homologs of polyhemeotic. *Mol. Cell Biol.* **17**, 2326-35.

Gutjahr, T., Frei, E., Spicer, C., Baumgartner, S., White, R. A. and Noll, M. (1995). The Polycomb-group gene, extra sex combs, encodes a nuclear member of the WD-40 repeat family. *EMBO J* **14**, 4296-4306.

Hanson, R. D., Hess, J. L., Yu, B. D., Ernst, P., van Lohuizen, M., Berns,

A., van der Lugt, N. M., Shashikant, C. S., Ruddle, F. H., Seto, M. and Korsmeyer, S. J. (1999). Mammalian Trithorax and polycomb-group homologues are antagonistic regulators of homeotic development. *Proc. Natl. Acad. Sci. USA* **96**, 14372-14377.

Hemenway, C. S., Halligan, B. W. and Levy, L. S. (1998). The Bmi-1 oncoprotein interacts with dinG and MPh2: the role of RING finger domains. *Oncogene* **16**, 2541-2547.

Hemenway, C. S., Halligan, B. W., Gould, G. C. and Levy, L. S. (2000). Identification and analysis of a third mouse Polycomb gene, MPc3. *Gene* **242**, 31-40.

Hobert, O., Jallal, B. and Ullrich, A. (1996). Interaction of Vav with ENX-1, a putative transcriptional regulator of homeobox gene expression. *Mol. Cell Biol.* **16**, 3066-3073.

Jacobs, J. J., Kieboom, K., Marino, S., DePinho, R. A. and van Lohuizen, M. (1999a). The oncogene and Polycomb-group gene bmi-1 regulates cell proliferation and senescence through the ink4a locus. *Nature* **397**, 164-168.

Jacobs, J. J., Scheijen, B., Voncken, J. W., Kieboom, K., Berns, A. and van Lohuizen, M. (1999b). Bmi-1 collaborates with c-Myc in tumorigenesis by inhibiting c-Myc-induced apoptosis via INK4a/ARF. *Genes Dev.* **13**, 2678-2690.

Jones, C. A., Ng, J., Peterson, A. J., Morgan, K., Simon, J. and Jones, R. S. (1998). The Drosophila esc and E(z) proteins are direct partners in polycomb group-mediated repression. *Mol. Cell. Biol.* **18**, 2825-2834.

Jurgens, G. (1985). A group of genes controlling the spatial expression of the bithorax complex in *Drosophila*. *Nature* **316**, 153-155.

Kanno, M., Hasegawa, M., Ishida, A., Isono, K. and Taniguchi, M. (1995). mel-18, a Polycomb group-related mammalian gene, encodes a transcriptional negative regulator with tumor suppressive activity. *EMBO J* **14**, 5672-5678.

Katoh-Fukui, Y., Tsuchiya, R., Shiroishi, T., Nakahara, Y., Hashimoto, N., Noguchi, K. and Higashinakagawa, T. (1998). Male-to-female sex reversal in M33 mutant mice. *Nature* **393**, 688-692.

Kerr, J. F., Gobe, G. C., Winterford, C. M. and Harmon, B. V. (1995). Anatomical methods in cell death. *Methods Cell Biol* **46**, 1-27.

Kessel, M. and Gruss, P. (1991). Homeotic transformations of murine vertebrae and concomitant alteration of Hox codes induced by retinoic acid. *Cell* **67**, 89-104.

Laible, G., Wolf, A., Dorn, R., Reuter, G., Nislow, C., Lebersorger, A., Popkin, D., Pillus, L. and Jenuwein, T. (1997). Mammalian homologues of the Polycomb-group gene Enhancer of zeste mediate gene silencing in Drosophila heterochromatin and at S. cerevisiae telomeres. *EMBO J* **16**, 3219-3232.

LaJeunesse, D. and Shearn, A. (1996). E(z): a polycomb group gene or a trithorax group gene? *Development* **122**, 2189-2197.

Lessard, J., Schumacher, A., Thorsteinsdottir, U., van Lohuizen, M., Magnuson, T. and Sauvageau, G. (1999). Functional antagonism of the Polycomb-Group genes eed and Bmi1 in hemopoietic cell proliferation. *Genes Dev.* **13**, 2691-2703.

Ng, J., Hart, C. M., Morgan, K. and Simon, J. A. (2000). A Drosophila ESC-E(Z) protein complex is distinct from other polycomb group complexes and contains covalently modified ESC. *Mol. Cell. Biol.* **20**, 3069-3078.

Nomura, M., Takihara, Y. and Shimada, K. (1994). Isolation and characterization of retinoic acid-inducible cDNA clones in F9 cells: one of the early inducible clones encodes a novel protein sharing several highly homologous regions with a Drosophila polyhomeotic protein. *Differentiation* **57**, 39-50.

Orlando, V., Jane, E. P., Chinwalla, V., Harte, P. J. and Paro, R. (1998). Binding of trithorax and Polycomb proteins to the bithorax complex: dynamic changes during early Drosophila embryogenesis. *EMBO J.* **17**, 5141-5150.

Paro, R. (1995). Propagating memory of transcriptional states. *Trends Genet.* **11**, 295-298.

Pearce, J. J., Singh, P. B. and Gaunt, S. J. (1992). The mouse has a Polycomb-like chromobox gene. *Development* **114**, 921-929.

Pirotta, V. (1997). PcG complexes and choromatinb silencing. *Curr. Opin. Genet. Dev* **7**, 249-258.

Satijn, D. P., Olson, D. J., van der Vlag, J., Hamer, K. M., Lambrechts, C., Masselink, H., Gunster, M. J., Sewalt, R. G., van Driel, R. and Otte, A. P. (1997). Interference with the expression of a novel human polycomb protein, hPc2, results in cellular transformation and apoptosis. *Mol. Cell. Biol.* **17**, 6076-6086.

Satijn, D. P. and Otte, A. P. (1999). Polycomb group protein complexes: do different complexes regulate distinct target genes? *Biochim. Biophys. Acta* **1447**, 1-16.

Schoorlemmer, J., Marcos-Gutierrez, C., Were, F., Martinez, R., Garcia, E., Satijn, D. P., Otte, A. P. and Vidal, M. (1997). Ring1A is a transcriptional repressor that interacts with the Polycomb-M33 protein and is expressed at rhombomere boundaries in the mouse hindbrain. *EMBO J.* **16**, 5930-5942.

Schumacher, A., Faust, C. and Magnuson, T. (1996). Positional cloning of a global regulator of anterior-posterior patterning in mice. *Nature* **384**, 648.

Sewalt, R. G., van der Vlag, J., Gunster, M. J., Hamer, K. M., den Blaauwen, J. L., Satijn, D. P., Hendrix, T., van Driel, R. and Otte, A. P. (1998). Characterization of interactions between the mammalian polycomb-group proteins Enx1/EZH2 and EED suggests the existence of different mammalian polycomb-group protein complexes. *Mol. Cell. Biol.* **18**, 3586-3595.

Shao, Z., Raible, F., Mollaaghababa, R., Guyon, J. R., Wu, C. T., Bender, W. and Kingston, R. E. (1999). Stabilization of chromatin structure by PRC1, a Polycomb complex. *Cell* **98**, 37-46.

Simon, J., Bornemann, D., Lunde, K. and Schwartz, C. (1995). The extra sex combs product contains WD40 repeats and its time of action implies a role distinct from other Polycomb group products. *Mech. Dev.* **53**, 197-208.

Strouboulis, J., Damjanovski, S., Vermaak, D., Meric, F. and Wolffe, A. P. (1999). Transcriptional repression by XPc1, a new Polycomb homolog in Xenopus laevis embryos, is independent of histone deacetylase. *Mol. Cell. Biol.* **19**, 3958-3968.

Struhl, G. and Brower, D. (1982). Early role of the esc+ gene product in the determination of segments in Drosophila. *Cell* **31**, 285-292.

Tagawa, M., Sakamoto, T., Shigemoto, K., Matsubara, H., Tamura, Y., Ito, T., Nakamura, I., Okitsu, A., Imai, K. and Taniguchi, M. (1990). Expression of novel DNA-binding protein with zinc finger structure in various tumor cells. *J. Biol. Chem.* **265**, 20021-20026.

Takihara, Y., Tomotsune, D., Shirai, M., Katoh-Fukui, Y., Nishii, K., Motaleb, M. A., Nomura, M., Tsuchiya, R., Fujita, Y., Shibata, Y., Higashinakagawa, T. and Shimada, K. (1997). Targeted disruption of the mouse homologue of the Drosophila polyhomeotic gene leads to altered anteroposterior patterning and neural crest defects. *Development* **124**, 3673-3682.

Tie, F., Furuyama, T. and Harte, P. J. (1998). The Drosophila Polycomb Group proteins ESC and E(Z) bind directly to each other and co-localize at multiple chromosomal sites. *Development* **125**, 3483-3496.

van der Lugt, N. M., Domen, J., Linders, K., van Roon, M., Robanus-Maandag, E., te Riele, H., van der Valk, M., Deschamps, J., Sofroniew, M., van Lohuizen, M. et al. (1994). Posterior transformation, neurological abnormalities, and severe hematopoietic defects in mice with a targeted deletion of the bmi-1 proto-oncogene. *Genes Dev.* **8**, 757-769.

van der Lugt, N. M., Alkema, M., Berns, A. and Deschamps, J. (1996). The Polycomb-group homolog Bmi-1 is a regulator of murine Hox gene expression. *Mech. Dev.* **58**, 153-164.

van der Vlag, J. and Otte, A. P. (1999). Transcriptional repression mediated by the human polycomb-group protein EED involves histone deacetylation. *Nat. Genet.* **23**, 474-478.

van Lohuizen, M. (1999). The trithorax-group and polycomb-group chromatin modifiers:implications for disease. *Curr. Opin. Genet. Dev* **9**, 355-361.

van Lohuizen, M., Tijms, M., Voncken, J. W., Schumacher, A., Magnuson, T. and Wientjens, E. (1998). Interaction of mouse polycomb-group (Pc-G) proteins Enx1 and Enx2 with Eed: indication for separate Pc-G complexes. *Mol. Cell. Biol.* **18**, 3572-3579.

van Lohuizen, M., Verbeek, S., Scheijen, B., Wientjens, E., van der Gulden, H. and Berns, A. (1991a). Identification of cooperating oncogenes in E mu-myc transgenic mice by provirus tagging. *Cell* **65**, 737-752.

van Lohuizen, M., Frasch, M., Wientjens, E. and Berns, A. (1991b). Sequence similarity between the mammalian bmi-1 proto-oncogene and the Drosophila regulatory genes Psc and Su(z)2. *Nature* **353**, 353-355.

Wilkinson, D. G. (1992). *In Situ Hybridization: A Practical Approach*. Oxford, Oxford University Press.

Yu, B. D., Hanson, R. D., Hess, J. L., Horning, S. E. and Korsmeyer, S. J. (1998). MLL, a mammalian trithorax-group gene, functions as a transcriptional maintenance factor in morphogenesis. *Proc. Natl. Acad. Sci. USA* **95**, 10632-10636.